Chapter 5. Synthesis, organo-functionalization, and catalytic properties of tungsten oxide nanoparticles as heterogeneous catalyst for oxidative cleavage of oleic acid as a model fatty acid into diacids

Amir Enferadi-Kerenkan [1], Aimé Serge Ello [1, 2], and Trong-On Do [1*]

1. Department of Chemical Engineering, Université Laval, Québec, G1V 0A6, Canada.
2. Laboratoire de Chimie Physique, Université Félix Houphouët-Boigny de Cocody, 22 bp 582 Abidjan, Cote d'Ivoire.

Industrial & Engineering Chemistry Research, 2017, 56 (38), 10639-10647.

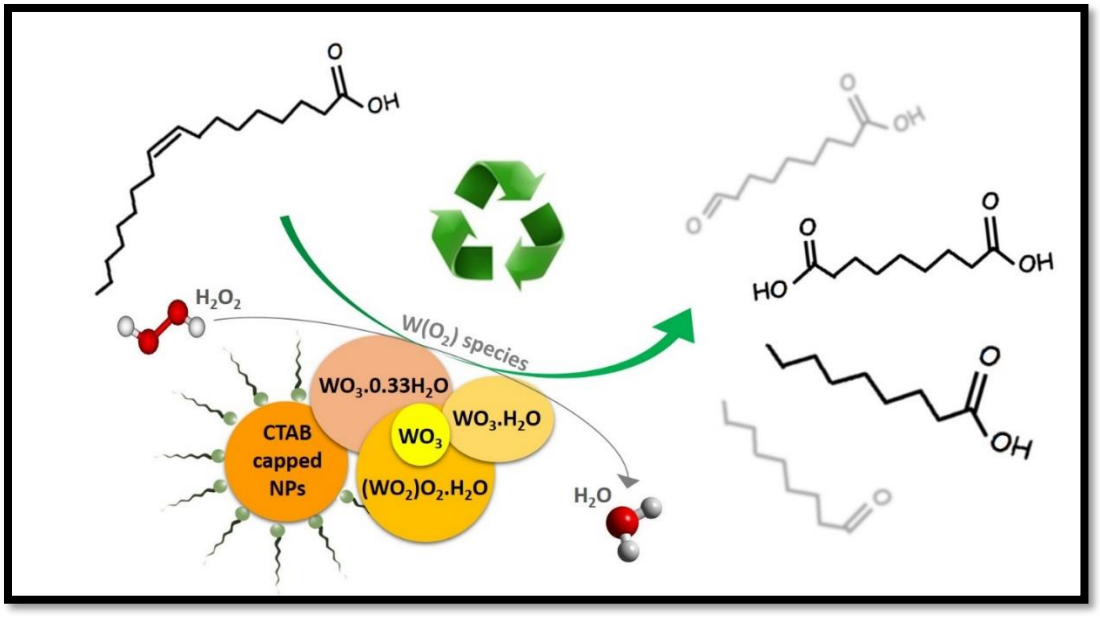

Résumé

Une série de nanoparticules d'oxyde de tungstène (NPs) a été synthétisée par une approche verte et directe exploitant la poudre de tungstène nu comme précurseur. Les NPs synthétisées ont été encore organo-fonctionnalisées par le bromure de cétyltriméthylammonium (CTAB) afin d'ajuster l'état de leur surface et d'améliorer leur compatibilité avec l'oxydation biphasique des huiles végétales avec H_2O_2. Simplement, différentes structures d'oxyde de tungstène ont été observées, ceux-ci ont été caractérisées par XRD, FTIR, TGA, TEM, N_2 isothermes d'adsorption / désorption, et l'analyse du potentiel zêta. Tous les nanocatalyseurs synthétisés ont pu convertir complètement l'acide oléique, et le rendement le plus élevé de la production du diacide désiré (acide azélaïque), ~ 80%, a été atteint par l'optimisation de la quantité de CTA^+ sur la surface du nanocatalyseur, ce qui montrent une excellente activité par rapport aux divers travaux signalés. Grâce à l'organo-fonctionnalisation, ce catalyseur tolérant à l'eau ne présentait pas de lixiviation significative aussi bien qu'une récupération pratique et une réutilisation régulière sans diminution notable de l'activité, au moins jusqu'à quatre cycles.

Abstract

A series of tungsten oxide nanoparticles (NPs) has been synthesized via a green and straightforward approach exploiting bare tungsten powder as precursor. The synthesized NPs were further organo-functionalized by cetyltrimethylammonium bromide (CTAB) in order to adjust their surface state and enhance their compatibility with biphasic oxidation of vegetable oils with H_2O_2. Simply, different structures of tungsten oxide were observed, which were characterized by XRD, FTIR, TGA, TEM, N_2 adsorption/desorption isotherms, and zeta potential analysis. All the synthesized nanocatalysts could fully convert oleic acid, and the highest yield of production of the desired diacid (azelaic acid), ~80 %, was achieved by optimization of the CTA^+ amount on the nanocatalyst's surface, which show excellent activity compared to the reported heterogeneous works. Thanks to the organo-functionalization, this water-tolerant catalyst exhibited no significant leaching, as well as convenient recovery and steady reuse without a noticeable decrease in activity, at least up to four cycles.

5.1 Introduction

Exploiting the synthetic capabilities of nature in oils and fats of vegetable and animal origin has rendered using these renewable raw materials one of the key aspects of sustainable chemistry. Oleic acid (C18:1), the most widely distributed and abundant unsaturated fatty acid (UFA) in natural oils and fats [338,29], can be oxidatively cleaved to produce azelaic (C9 diacid) and pelargonic (C9 monoacid) acids, which are rare in natural resources but very attractive materials, in particular the first one, for preparation of numerous products such as polymers (nylon 6:9), adhesives, biodegradable lubricants, corrosion inhibitors, anti-acneic agent for cosmetics, perfumes, and resins [2,4,1,5,3]. Currently, this reaction is carried out in industry via ozonolysis, which, nowadays, has been converted to a controversial challenge due to the hazardous problems associated with use of ozone. Employing an eco-friendlier oxidant requires an active catalyst to be employed, as well.

Efforts in this context have focused on transition metals like Mo [3], Au [1], Mn, Cr [339], Co [339,54], Fe [56,55], Ru [60,59,87,58,57], and W [64,2,65,340,341,48,61,62,3], as catalytic core, in homogeneous and heterogeneous forms. These have been thoroughly reviewed in our recent review paper [91]. While the use of homogeneous catalysts has been well reported, curiously, heterogeneous ones have been scarcely investigated, probably due to the, often, much lower yields obtained with the latter. Hydrogen peroxide has been always an interesting benign oxidant for oxidation of olefins, especially when its use is associated with employing phase transfer agents via functionalization of catalyst surface to improve compatibility of the aqueous oxidant and organic substrate. Although this could generally increase the efficiency of oxidation of UFAs [64,2,65,341,62,3], the major drawback is that the used catalytic system is not fully recoverable.

Among all the transition metals, tungsten has attracted a great deal of interest in oxidation of UFAs, mostly in W-based complex form and homogeneous catalysis [91,45,39]. Solid W-based catalysts, however, include a variety of chemical structures arising from the distinct inherent properties of tungsten; varying oxidation states from -2 to +6 [120,121] has led to several WO_x (x mainly between 2 and 3). The most common is tungsten trioxide, which in turn, includes hydrated ($WO_3.nH_2O$) and anhydrous (WO_3) forms. Moreover, peroxotungstic acid is another interesting

structure that has shown great catalytic potential, particularly in oxidation reactions [342-345]. Formation of these different phases are very sensitive to synthesis conditions [346-349], so, choice of a unique synthesis method that can produce all the phases is of importance. Oxidative dissolution of tungsten metal or tungstic acid in H_2O_2 was proposed by Kudo et al. to synthesize peroxotungstic acid [350-352], and then was modified to synthesize some other tungsten oxide structures [353-355,349]. Recently, Ozin et al. developed this method to produce nanoparticles and thin films of tungsten oxide, as well as some other metal oxides [356].

In this work, different structures of tungsten oxide like $[(WO_2)O_2.H_2O]$, WO_3, $WO_3.0.33H_2O$, and $WO_3.H_2O$ were synthesized via oxidative dissolution of micrometer-scale bare W powder, and then, these materials were examined in the oxidative cleavage of oleic acid. In order to tune hydrophobicity/hydrophilicity properties of the surface and improve compatibility of the solid catalysts with the organic substrate and aqueous oxidant, the nanocatalysts were organo-functionalized with different amounts of cetyltrimethylammonium bromide (CTAB), a well-known cationic surfactant. Employing a simple and green synthesis method, that exploits cheap W powder as a precursor, avoided using time- and energy-consuming operations such as thermal treatment in autoclave and purification, organic solvents, metal salts, and/or coordination compounds, which are commonly required in prior reported synthesis methods.

5.2 Experimental

5.2.1 Synthetic details and characterization

Tungsten oxide NPs were prepared by simple dispersion of metallic tungsten powder (1.0 g) (APS 1-5 μm, purity 99.9%, Alfa Aesar Co.) in deionized H_2O (10 mL), followed by addition of H_2O_2 (10 mL, aqueous solution, 30 %, Fisher Scientific Co.) dropwise. The latter was done at 0 °C by keeping the reaction vessel in an instant ice bath. The oxidative dissolution process is very exothermic, therefore must be done attentionally under a well-ventilated fume hood. After 4 *h*, an almost colorless (very slightly light yellow) and clear solution was formed (solution **A**). This solution was, then, allowed to precipitate through two different ways: (i) it was slowly evaporated at room temperature (RT) for 3 days (sample I), followed by calcination at 600 °C for 3 *h* (heating rate: 4 °C/min) under air to obtain sample II, or (ii) it was heated to 120 °C for 4 *h* in the absence of CTAB (sample III) and in the presence of CTAB (technical grade, Fisher Scientific Co.) with

molar CTAB/W ratios of 0.1, 0.25, and 0.5 added to the solution just before heating (samples IV, V and VI, respectively). Solid products were separated using a centrifuge at 8000 rpm, washed thoroughly with water and ethanol, and dried at 60 °C overnight (16 *h*). The used 1 g W gave ~ 1.1-1.6 g products. The synthesized samples were characterized by XRD, FTIR, TGA and DTA, TEM, zeta potential analyzer, and BET surface area measurement. Section 5.5.1 in Supporting Information explains characterization equipment and methodologies.

5.2.2 Catalytic test

The reactions were carried out in a 50-mL, round-bottom flask under a batch-wise constant temperature and constant pressure mode. This reactor was equipped with a condenser, a magnetic stirrer, and an oil bath. Typically, the reaction feed included 1 g oleic acid (≥ 99%, Sigma-Aldrich Co.), 4 mL H_2O_2, 7.5 mL tert-butanol (≥ 99.0%, Sigma-Aldrich Co.) as solvent. After adding 0.45 g catalyst, the flask was put in the oil bath which was previously heated and maintained at constant temperature of 120 °C. During reaction, the reactor was continuously agitated with magnetic stirrer (agitation rate ~ 400 rpm). After 5 *h* reaction, the catalyst was separated using centrifuge at 8000 rpm and recovered via washing with ethanol and water several times and drying at 60 °C overnight to be used in the next catalytic cycle. The products mixture, then, underwent a derivatization reaction, in which the expectedly produced azelaic and pelargonic acids, and possibly unreacted oleic acid were converted to their corresponding methyl esters according to Metcalfe et al. derivatization procedure [334,335], in order to be prepared for GC-MS analysis.

Analysis of the reaction products by GC-MS has been explained in section 5.5.2 of the Supporting Information, covering detailed information about sample preparation prior to injection (section 5.5.2.1), quantitative analysis (section 5.5.2.2), and GC-MS specifications (section 5.5.2.3).

5.3 Results and discussions

5.3.1 Catalysts synthesis and characterization

Simply taking W powder, adding H_2O_2, and then by just altering the temperature of thermal treatment and/or adding a surfactant, different catalytically interesting structures of tungsten oxide

were achieved. Table 5.1 summarizes the synthesis conditions and prepared samples and shows their obtained crystalline phases and chemical structures.

Table 5.1. Synthesis conditions and prepared samples.

		Synthesis [1]			
Sample	CTAB/W molar ratio	T (°C)	t (h)	Crystalline phase	Chemical structure
I	-	RT [2]	72	Monoclinic	$(WO_2)O_2.H_2O$
II [3]	-	600	3	Monoclinic	WO_3
III	-	120	4	Orthorhombic	$WO_3.0.33H_2O$ & $WO_3.H_2O$
IV	0.1	120	4	Orthorhombic	$WO_3.0.33H_2O$ >> $WO_3.H_2O$
V	0.25	120	4	Orthorhombic	$WO_3.0.33H_2O$ >>> $WO_3.H_2O$
VI	0.5	120	4	Orthorhombic	$WO_3.0.33H_2O$

1. Synthesis conditions: initial amounts of W elemental powder (1 g), H_2O (10 ml), H_2O_2 (10 ml), CTAB (0.20, 0.50, and 0.99 g for samples IV, V, and VI, respectively).
2. RT: room temperature
3. Sample II: Sample I followed by calcination at 600 °C for 3 *h*.

5.3.1.1 Crystalline structural features

Fundamentally, oxidative dissolution of W powder in H_2O_2 gives an almost colorless and strongly acidic solution containing amorphous peroxotungstic acid particles, for which, the empirical formula of $WO_3.xH_2O_2.yH_2O$ ($0.05 \leq x \leq 1$ and $3 \leq y \leq 4$) has been suggested in literature [357,355]. This solution, denoted as **A**, then underwent different crystallization approaches to achieve the catalytically desired structures of tungsten oxide. XRD patterns of the synthesized samples are shown in Figure 5.1. While rapid evaporation of solution **A**, expectedly, gave amorphous tungsten oxide, interesting structure of peroxotungstic acid or hydrated tungsten peroxide [$(WO_2)O_2.H_2O$], which contains active oxidizing agent of tungsten-peroxo, was obtained by slowly evaporation of the solution at RT for 3 days (Sample I). Its well-defined peaks (Figure 5.1 a) could be precisely and purely indexed on monoclinic structure, the most stable phase of tungsten oxides at RT [358], in accordance with PDF no. 50-0233 of ICDD library of spectra. Pecquenard et al. [355], who are the pioneers in structural investigations of hydrated tungsten peroxide, reported that [$(WO_2)O_2.H_2O$] can be obtained only after heating at 120 °C, while at RT a more hydrated phase [$(WO_2)O_2.H_2O$].nH_2O is formed. Our synthesis method, however, made the

formation of [$(WO_2)O_2.H_2O$] at RT in 3 days possible. Anhydrous WO_3, another catalytically interesting structure, was obtained by decomposition and annealing of tungsten peroxide (sample I) [359,360] via calcination at 600 °C (sample II, Figure 5.1 b). Presence of {200}, {002}, and {020} reflections confirm that the obtained yellow powder was mainly composed of monoclinic WO_3 (PDF no. 83-0950).

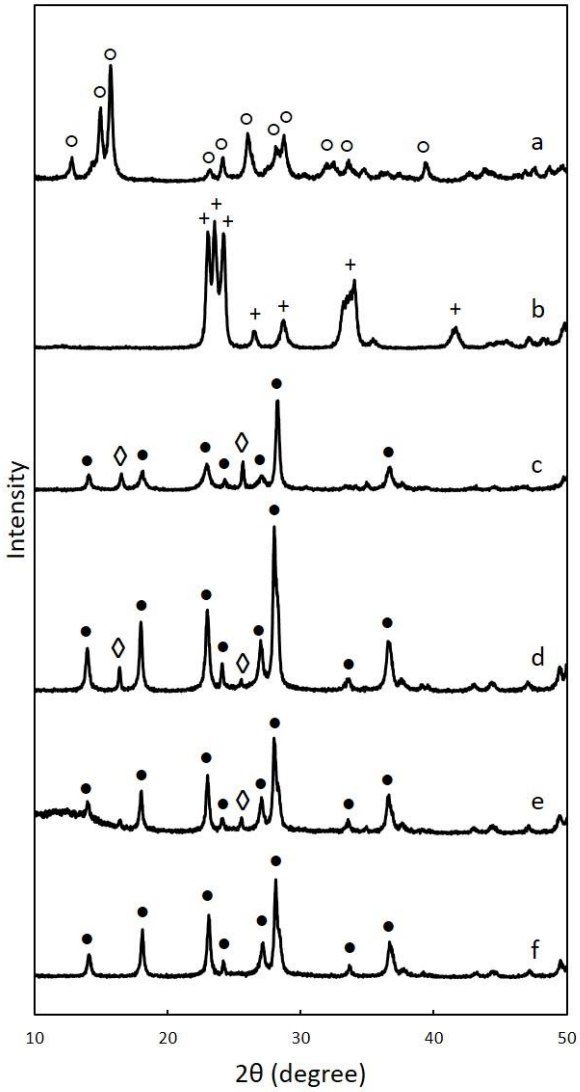

Figure 5.1. XRD patterns of (a) sample I, (b) sample II, (c) sample III, (d) sample IV, (e) sample V, and (f) sample VI. (o) $(WO_2)O_2.H_2O$ (PDF no. 50-0233), (+) WO_3 (PDF no. 83-0950), (●) $WO_3.0.33H_2O$ (PDF no. 35-0270), and (◊) $WO_3.H_2O$ (PDF no. 43-0679).

Given the importance of associated water molecules of WO_3 [122], hydrated tungsten oxides were also synthesized (samples III-VI) via execution of higher thermal treatment (at 120 °C) on solution **A**, instead of the slow evaporation at RT, which resulted in much shorter crystallization time, as well as, changing the crystalline structure from monoclinic to orthorhombic (in comparison with samples I and II). Heating leads to quick decomposition of the water-soluble amorphous particles of solution **A** and production of insoluble solids with crystalline structures. XRD pattern of sample III (Figure 5.1 c) shows that it is composed of $WO_3.0.33H_2O$ (PDF no. 35-0270) and $WO_3.H_2O$ (tungstite) (PDF no. 43-0679). The high intensity of the peaks at $2\theta = 28.3$, 23.1, 36.8, and 18.1 degree demonstrates domination of the less hydrated phase, however, the main reflections of tungstite at $2\theta = 25.7$ ({111}) and $2\theta = 16.5$ ({020}) are also observed with less intensity. Both phases possess orthorhombic crystalline structure.

Adding CTAB to the synthesis mixture reinforced the dominance of $WO_3.0.33H_2O$, evidence for which is the gradual diminishing of the intensities of two mentioned peaks of tungstite, in samples IV, V, and VI (Figure 5.1 d, e, and f), insofar as 100% pure $WO_3.0.33H_2O$ (PDF no. 35-0270) was obtained in sample VI (CTAB/W = 0.25) (Figure 5.1 f). This phase of tungsten oxide has been emphasized as very sensitive to the synthesis conditions [349,361]. The reported synthesis methods in the literature are considerably more complicated and time-consuming than the presented method. In fact, a role of structure directing agent (SDA) can be well considered for CTA^+ cations in this synthesis method that directed the crystals to form pure orthorhombic $WO_3.0.33H_2O$ structure in sample VI.

5.3.1.2 Spectral analysis

FTIR analysis was employed to learn more about the composition of the organic part of the samples as well as different available tungsten bonds in crystalline structures of the samples. FTIR spectra of the samples are shown in Figure 5.2 and assignments of the considerable absorption bands are listed in Table 5.3 (Supporting Information).

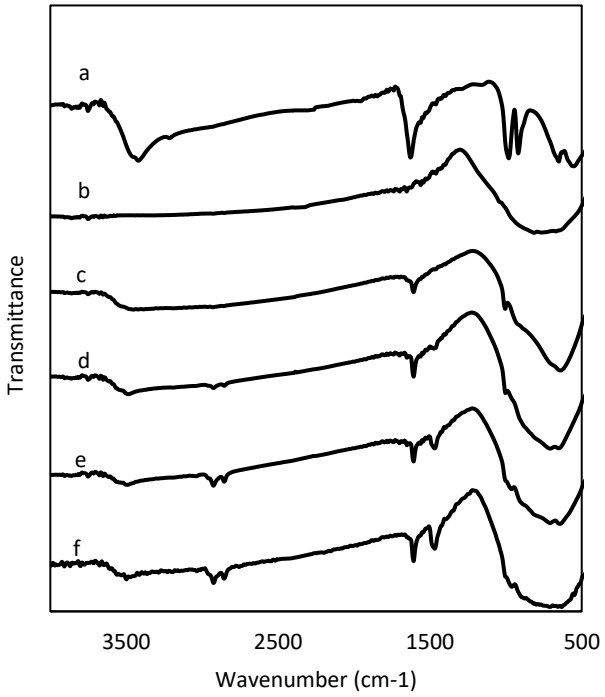

Figure 5.2. FTIR spectra of (a) sample I, (b) sample II, (c) sample III, (d) sample IV, (e) sample V, and (f) sample VI.

All the samples exhibit a strong peak located at 641-672 cm^{-1} which is assigned to stretching vibration of bridging oxygen atom between two tungsten atoms ν(W–O–W) [362,122,363,364]. Generally, spectra of all the synthesized crystalline powders are very similar in the low-frequency region, except for sample I that shows two more peaks at 548 and 919 cm^{-1}. These peaks, which are respectively assigned to tungsten–peroxo ($W(O)_2$) and peroxo (O–O) groups, are typical vibration bands of peroxotungstic acid [363]. The peak located at 950-1004 cm^{-1}, which is sharp in sample I and poorly resolved in other hydrated tungsten oxides (samples III-VI), is ascribed to the stretching mode of the terminal W=O double bond [365,122,363,366].

Obviously, the peak(s) between 600 and 900 cm^{-1} is wider in the presence of CTA^+ cations (from sample IV to VI). The reason is the emergence of some peaks corresponding to $RN(CH_3)_3^+$ at 910-970 cm^{-1} [367] and merging with the previous peaks. The spectra of CTAB-assisted synthesized samples (samples IV-VI) exhibit some additional peaks in the higher frequency region,

where the vibration of organic compounds, as well as water molecules, are expected to appear. According to the literature, the peak at 1467 cm^{-1} can be attributed to $RN(CH_3)_3^+$ and the peaks at 2850 and 2927 cm^{-1} can be assigned to stretching vibrations of methyl ($–CH_3$) and/or methylene ($–(CH_2)–$) groups [367]. These peaks, although weak in sample IV, their intensities increase with increasing CTAB content in the synthetic mixture for samples V and VI. The hydrated crystalline structures (samples I and III-VI) demonstrate a peak at 1606-1622 cm^{-1} and a peak at 3421-3491 cm^{-1}, which come from, respectively, bending and stretching vibrations of H_2O molecules [362,122,363].

5.3.1.3 Thermal analysis

Thermogravimetric analysis (TGA) and differential thermal analysis (DTA) curves of the synthesized samples are illustrated in Figure 5.3. Expectedly, anhydrous WO_3 (sample II) showed no essential weight loss during the thermal analysis up to 800 °C, and therefore, its curve is not included in Figure 5.3.

Initially, thermal analysis of sample III composed of only water and WO_3 (Figure 5.3 b) indicates that the water molecules were expelled from the tungsten oxide structure at temperatures less than about 300 °C. Above this temperature, the sample's weight, belonging to WO_3 portion, remained constant. Gradual expulsion of water that happened over a relatively wide temperature range ($25 < T < 300$ °C) comes from two main groups of the departed water molecules; (i) adsorbed and weakly bonded molecules that are normally released at $T < 200$ °C, and (ii) HO and HO-O groups and strongly bonded molecules which due to the inherent tendency of tungsten oxide to keep the water of hydration even at high temperatures, release at $200 < T < 300$ °C as the reaction products of W-OH and W-OOH condensation [353,354]:

$$2[-W-OH] + 2[-W-OOH] \rightarrow 2[W-O-W] + 2H_2O + O_2 \qquad (5.1)$$

Presence of abundant peroxide groups in sample I changed the behavior of departure of water molecules (Figure 5.3 a); its first weight loss at about 110 °C, similarly, comes from the departure of weakly bonded water molecules, however, more strongly bonded molecules departed the structure along with the peroxide group at about 220 °C, which resulted in more abrupt departure and greater weight loss compared to the other samples.

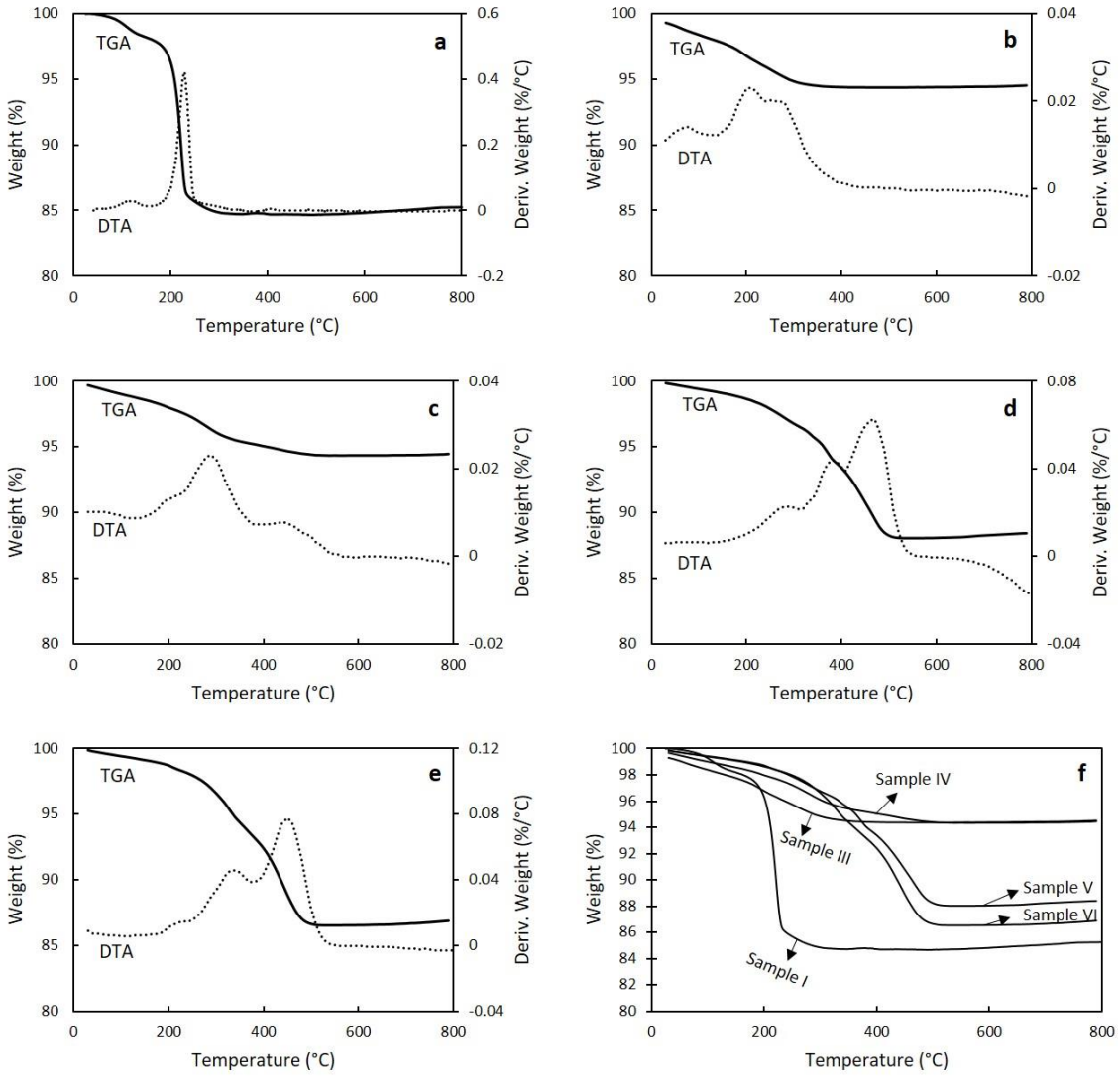

Figure 5.3. (a-e): TGA and DTA curves of (a) sample I, (b) sample III, (c) sample IV, (d) sample V, and (e) sample VI. (f): all the TGA curves.

In the high temperature region (T > 300 °C), an additional weight loss is obtained only for the CTA^+ containing samples (Figure 5.3 c-e). This weight loss, which increases with CTA^+ content in the synthesis mixture, corresponds to oxidation and consequent removal of CTA^+ molecules that capped the surfaces of tungsten oxides. Quantitatively, 1.7, 8.7, and 10.0% weight losses (in 300 < T < 500 °C) were obtained for samples IV, V, and VI, in which CTAB/W molar ratios of 0.1, 0.25, and 0.5 had been used in the synthetic solution, respectively. Differential thermal analysis indicated

that removal of CTA^+ took place at two main sub-temperature range: (i) 300 < T < 350 °C and (ii) 440 < T < 470 °C.

Figure 5.3 f compares TGA curves of all the samples together. As can be seen, at all temperatures lower than 300 °C the curves of CTA^+-capped samples (samples IV-VI) stay on top of that of sample III. This confirms lower water contents in the structures of samples IV-VI, concurring with the result of XRD.

5.3.1.4 Other aspects of the synthesized samples

High concentration of charged species and functional groups (and their probable ionization) in the synthesis medium [356], as well as not using autoclave in the employed pseudo-hydrothermal synthesis method could mainly affect the morphologies and surface areas of the resultant solids.

Figures 5.4 and 5.5 display representative TEM images of the samples. NPs of $(WO_2)O_2.H_2O$ (sample I, Figure 5.4 a and b) tend to form into irregular-shaped substructure due to the high concentration of peroxo groups on their surface. Firstly, the presence of many hydrogen ions in the precursor solution has been reported that increases the aggregation of tungsten oxide NPs [368]. Moreover, control of morphology to form a stable coordinated structure in the presence of H_2O_2 could be difficult due to the chelating feature of peroxo ligands $[O_2]^{2-}$ [349]. It makes more sense given the fact that no autoclave was used for hydrothermal treatment. Indeed, this chelating property of $[O_2]^{2-}$ ligands has been well-thought-out as the fountainhead of H_2O_2 role in the synthesis [349], which led to complete dissolution of WO_3 in hydrogen peroxide and formation of transparent tungsten peroxide solution, while WO_3 is not soluble in water.

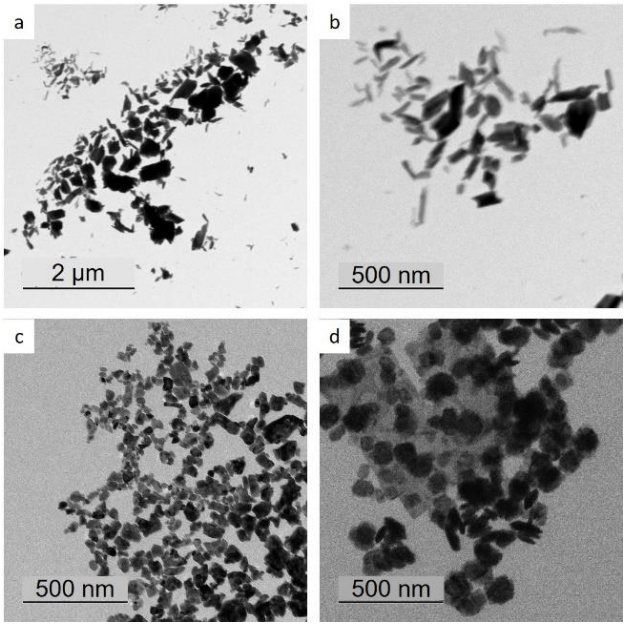

Figure 5.4. TEM images of (a) and (b) sample I (with different magnifications), (c) sample II, and (d) sample III.

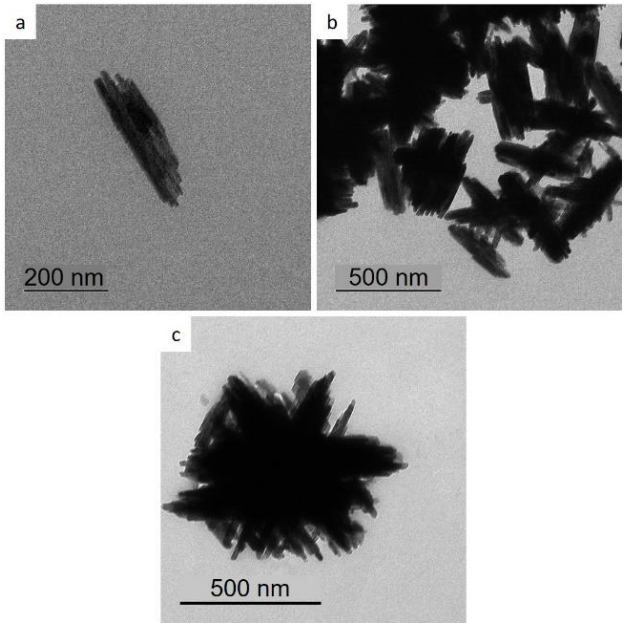

Figure 5.5. TEM images of (a) sample IV, (b) sample V, and (c) sample VI.

Calcining at 600 °C and removal of hydrogen peroxide, monoclinic WO_3 NPs with platelet-like morphology with an average size of ≈ 40 nm were obtained (sample II, Figure 5.4 c). Thermal

treatment at higher temperature had little influence on the overall morphology of the product; as shown in Figure 5.4 d, the typical structure of sample III is a mixed morphology of nanoplatelet and nanorod, most likely due to the coexistence of two crystalline phases $WO_3.0.33H_2O$ and $WO_3.H_2O$, and the platelet structure is somehow similar to sample II.

Adding CTAB to the synthesis medium, nanoneedle aggregates were formed (Figure 5.5), a typical morphology for $WO_3.0.33H_2O$ that had been obtained before via more complicated and longer procedures [361,349]. Changing the amount of CTAB, however, did not have a significant effect on the morphology of the products. Only, it seems that at higher concentration of CTAB the particles showed slightly more tendency to aggregate. As consequence, the specific surface area decreased from 17 m^2/g in sample III to about 4 m^2/g in sample VI. Table 5.4 in Supporting Information lists the BET surface areas of the samples. Higher surface area of sample II (~29 m^2/g) compared to the other samples highly likely arises from its calcination at a higher temperature, which removed all the surface functional groups, and therefore its NPs strongly avoid aggregation, as can be seen in its TEM image (Figure 5.4 c).

Our efforts to organo-functionalize the tungsten oxides with anionic surfactants (e.g. acetic and valeric acids, instead of CTAB) failed (as TGA and FTIR analyses confirmed), because the anionic functional groups at the head of these surfactants were repelled by negatively charged surface of tungsten oxide. Evidence for this negative charge was obtained by measuring zeta potential of the NPs dispersed in solution **A** (without CTAB, pH 1.6-1.8, Figure 5.6). The available negatively charged species on the surface mainly consists of peroxo (O_2^{2-}) and hydroxyl group (OH^-) (see Figure 5.2 and well-resolved absorption band of peroxo at 919 cm^{-1}. Presence of such band in Figure 5-2 c, although very weak, confirms that even after heating at 120 °C, there is still some O_2^{2-} ligands on the surface, while $W(O_2)$ absorption band (548 cm^{-1}) had been vanished).

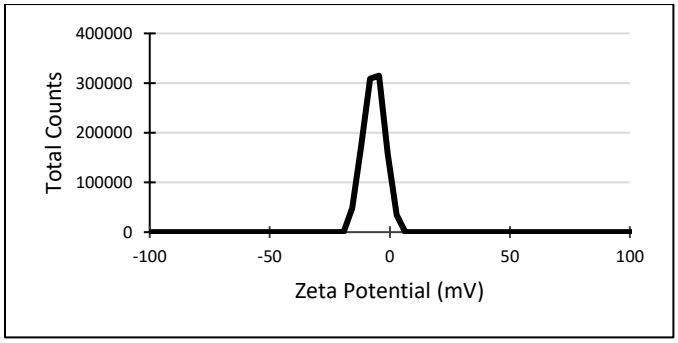

Figure 5.6. Surface zeta potential distribution of tungsten oxide NPs dispersed in the synthesis solution without adding CTAB at pH 1.6-1.8.

5.3.2 Catalytic test results

Table 5.2 shows conversion of oleic acid and yields of production of azelaic and pelargonic acids (Y_{AA} and Y_{PA}, respectively) over different synthesized catalysts with H_2O_2 as oxidant after 5 *h* reaction at 120 °C (bath temperature). The catalytic test results presented are the average of at least 3 runs over each catalyst. See Supporting Information for more details about the quantitative analysis (section 5.5.2.2).

Table 5.2. Catalytic tests results (conversion of oleic acid and yields of production of desired products) and weight fractions of WO_3 in the catalysts as the assumed active sites.

Entry	Catalyst (tungsten oxide)	Chemical structure	WO_3 weight fraction in the catalyst (%) [1]	Conversion (%) [2]	Y_{AA} (%) [3]	Y_{PA} (%) [3]
1		-	-	41	2	4
2	Commercial	WO_3	-	91	10	18
3	Sample I	$(WO_2)O_2.H_2O$	84.9	100	71	67
4	Sample II	WO_3	100.0	100	41	39
5	Sample III	$WO_3.0.33H_2O$ & $WO_3.H_2O$	94.5	100	51	53
6	Sample IV	$WO_3.0.33H_2O$ >> $WO_3.H_2O$	94.3	100	39	37
7	Sample V	$WO_3.0.33H_2O$ >>> $WO_3.H_2O$	88.1	100	77	69
8	Sample VI	$WO_3.0.33H_2O$	86.5	100	60	64

1. Weight fraction of WO_3, assumed as active site (regardless of current vast challenges on nature of catalytic centers in metal oxide catalysis), was calculated from quantitative analysis of TGA data.
2. Reaction conditions: time: 5 h, temperature: 120 °C (bath temperature), solvent: tert-butanol, initial amounts of oleic acid: 1 g, t-butanol: 7.5 ml, H_2O_2: 4 ml, catalyst: 0.45 g, agitation rate ~ 400 rpm.
3. Y: Yield (molar), in this work, is defined as the amount of a product formed per total amount of oleic acid consumed (both in mole, Y_{AA}: yield of azelaic acid, Y_{PA}: yield of pelargonic acid).

5.3.2.1 Influence of different catalysts on the reaction

The first catalytic test was done without any catalyst (Table 5.2, entry 1); modest 41% conversion and tiny yields percentages (≤ 4%) confirmed that the benign used oxidant is not adequately efficient alone. To compare our catalysts activities with a standard condition, a commercial tungsten oxide (WO_3, 99.8%, Alfa Aesar Co.) was employed as a catalyst, also (entry 2), which although, significantly increased the conversion (~ 90%), the yields were still low (less than 20%). Compared to the commercial WO_3, our prepared tungsten oxides showed much better efficiencies (entries 3-8). Complete conversion of initial oleic acid was obtained for all the samples after 5 *h* reaction time, with high yields particularly for sample I, V, and VI.

The high catalytic efficiency of sample I (entry 3, 71 and 67% Y_{AA} and Y_{PA}, respectively) comes from the tungsten-peroxo (as seen by its XRD and FTIR) with a high concentration (as its TGA showed) in its structure [$(WO_2)O_2.H_2O$]. Such peroxo complexes have been mentioned in the literature that shoulder responsibility of advancing UFAs oxidative cleavage reactions [64,65,341,3]. Except sample I, other samples were composed of tungsten trioxide, in anhydrous (sample II) or hydrated (samples III-VI) forms. Sample II in spite of advantages of higher WO_3 content (Table 5.2) and surface area (Table 5.4), as well as more uniform morphology and smaller particle size (Figure 5.4), yielded lower compared to sample III (entries 4 and 5). The reason could be well ascribed to important role of the linked water molecules of sample III ($WO_3.0.33H_2O$ & $WO_3.H_2O$), which can increase in-situ production of instant tungsten-peroxo groups during the reaction. It has been shown that oxidation extent of tungsten trioxide in presence of H_2O_2 (to produce tungsten-peroxo) decreases with decreasing water content in its structure [122].

Samples IV-VI, however, did not generally comply with this trend (entries 6-8). As discussed in section 5.3.1.1, adding CTAB favored formation of the less hydrated phase ($WO_3.0.33H_2O$), and accordingly, it was expected that oxidative capabilities of the samples and, consequently, their catalytic efficiencies decrease by adding CTAB. But, except sample IV, the two other CTA^+-capped samples (V and VI) exhibited higher yields compared to sample III. The reason directly comes from the presence of CTA^+ which tunes surface state of the tungsten oxide, and greatly affects its catalytic activity. Samples IV-VI, despite very slight structural differences in crystallinity (Figure 5.1), morphology (Figure 5.5), and WO_3 content (Table 5.2), exhibited significantly different yields. The CTA^+ molecules that capped the hydrophilic surface of

$WO_3.0.33H_2O$ could make it partly hydrophobic, and hence, increased surface affinity to adsorb the organic substrate, oleic acid, molecules in the reaction medium. Admittedly, a higher concentration of oleic acid on the surface of the catalyst, where tungsten-peroxo species are accumulated, results in higher reactants collision and consequently increases the reaction efficiency (happened for samples V and VI). However, presence of long-chain CTA^+ on the surface is a double-edged sword; apart from the positive effect of hydrophobization, it would lead to a steric repulsion effect which, considering molecular geometry of CTA^+ and oleic acid, could prevent oleic acid to approach to the surface. The competition between these two positive and negative effects, which depends on the density of CTA^+ on surface, gives rise to the different yields obtained by samples IV, V, and VI; it seems that low density of CTA^+ in sample IV could not provide enough hydrophobicity, and the steric repulsion forces resulted in lower yields (entry 6), while at the higher density (sample VI), the provided hydrophobicity overcame the increase in steric repulsion effects resulting in higher yields (entry 8). The optimized density of CTA^+ on surface, giving 77% Y_{AA} (entry 7), was obtained when CTAB/W molar ration of 0.25 was used in the synthesis (sample V). The obtained reaction efficiencies in this work seem interesting when being compared with the previously reported heterogeneous catalytic oxidative cleavage of oleic acid [339,340,48].

Given the improved compatibility of the solid catalysts with reactants, resulting in deservedly ascribing a phase transfer role to the organo-functionalized tungsten oxides, further works are currently underway in our laboratory to reduce (or even eliminate) the reaction solvent.

5.3.2.2 Effects of temperature and time on the reaction

Sample V was subjected to investigate effect of reaction temperature and time. Employing a lower reaction temperature (bath temperature: 85 °C) resulted in slightly lower conversion (92%) and moderately lower Y_{AA} and Y_{PA} (49 and 47%, respectively). Since complete conversion of oleic acid was obtained at 120 °C, the temperatures higher than this, which would cause decomposition of hydrogen peroxide, were not tried. To study H_2O_2 loss during the reaction through catalytic or thermal decomposition, some catalytic tests without oleic acid were carried out, and then H_2O_2 loss was calculated by titrimetry. Results showed a 22% loss in absence of any catalyst and 30-70% in presence of the synthesized catalysts after 5 *h* reaction at 120 °C.

Employing shorter reaction times resulted in a significantly lower conversion. After 3 *h* reaction at 120 °C, over sample V, 58% of initial oleic acid was converted to azelaic and pelargonic acids with the yields of 62 and 59%, respectively. Longer reaction time (7.5 *h*) caused the yields to slightly reduce, most probably due to degradation of azelaic and pelargonic acids caused by prolonged heating in presence of catalyst [48]. Further works to optimize the reaction temperature and time for all the samples via kinetic studies are ongoing in our lab and will be presented in another article.

5.3.2.3 Recyclability of the catalysts

All the synthesized catalysts were recovered after the reactions and reused to examine their recyclability. Up to four cycles, they all showed more than 97% conversion without significant loss in the yields, except sample I which showed a considerable decrease in catalytic efficiency after the first cycle. Figure 5.7 compares the yields of production of azelaic acid in four cycles. Almost the same trend was obtained for Y_{PA}.

FTIR analysis was performed on the catalysts after each cycle to probe any change in their chemical structures. Except sample I, other catalysts exhibited almost the same FTIR patterns to their original spectra (Supporting Information, Figures 5.16 to 5.21) confirming that they essentially keep their chemical natures during the reaction. This chemical stability is because the catalysts had been already exposed to a thermal treatment at high temperatures (600 °C for sample II and 120 °C for sample III to VI) during the synthesis procedure. Whereas the structure of sample I, which had been synthesized at RT, was dramatically changed after the first cycle. Evidence for this was found in its FTIR analysis, before and after the reaction (Figure 5.16), as well as XRD analysis (Figure 5.22), where disappearance of corresponding peaks of $[(WO_2)O_2.H_2O]$, and instead, emerging the characteristic peaks of $WO_3.0.33H_2O$ (PDF no. 87-1203) imply decomposition of inter-crystalline tungsten-peroxo species during the reaction. This gives rise to the significant loss of catalytic efficiency of sample I after the first reaction cycle.

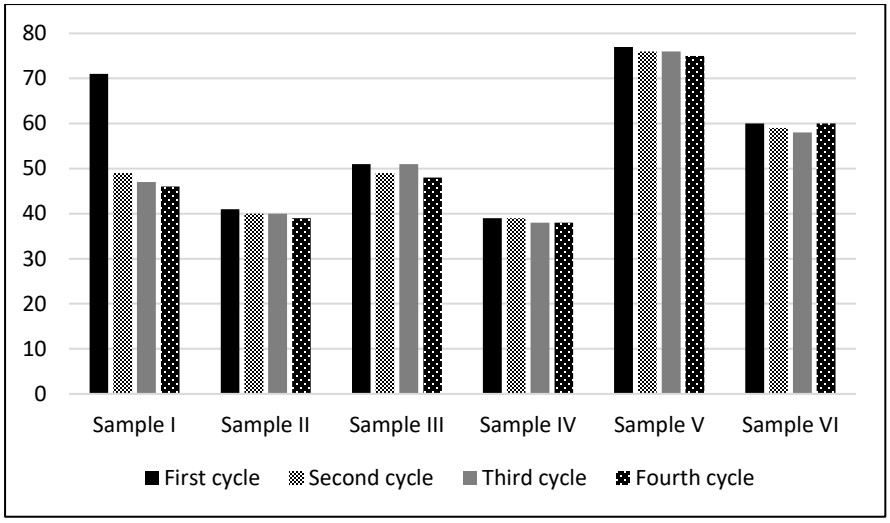

Figure 5.7. Recyclability of the synthesized catalysts; yields of production of azelaic acid over the synthesized catalysts in fourth cycles (reaction conditions: time: 5 h, temperature: 120 °C (bath temperature), solvent: tert-butanol, initial amounts of oleic acid: 1 g, t-butanol: 7.5 ml, H_2O_2: 4 ml, catalyst: 0.45 g, agitation rate: ~ 400 rpm).

In order to examine leaching of WO_3 species and truly heterogeneity of the reaction, a catalytic test was performed over sample V, which had given the highest yields, and stopped after 2.5 *h* of reaction. After cooling down and removal of catalyst, the reaction mixture was exposed to the reaction conditions for the remaining reaction time (2.5 *h*). In the second 2.5 *h*, conversion slightly increased (from 43% to 51%), as a result of oxidant ability in advancing the reaction alone (see entry 1 of Table 5.2), while changes in the yields were negligible. Moreover, for all the samples, weight loss of catalyst after each reaction cycle was exactly measured (Supporting Information, Table 5.5). Generally, the catalysts weight losses were less than ~ 2 %, with the minimum values, interestingly, obtained for the organo-functionalized catalysts (particularly samples V and VI), most likely because of hydrophobization effects making the CTA^+-capped catalysts more water-tolerant with less leaching of inherently hydrophilic active sites (WO_3). These results imply no significant leaching of active sites during the reaction.

5.4 Conclusions

A straightforward and green synthetic procedure, simply starting from cheap micrometer-scale W powder and adding H_2O_2, resulted in the formation of a clear solution of peroxotungstic species, which were then crystallized into different structures of tungsten oxide via altering temperature and/or adding CTAB. Given the potential of WO_x as oxidizing catalyst, all the synthesized catalysts were adequately efficient to fully convert oleic acid after 5 *h* reaction with H_2O_2 as a benign oxidant. Intriguingly, adding CTAB to the synthesis mixture, not only played a structure-directing role influencing the final product crystalline phase, but also stably capped the surfaces of tungsten oxide NPs resulting in an improved compatibility of the solid catalyst with the organic substrate and aqueous oxidant, and consequently, enhancing production yield of the desired azelaic acid up to just less than 80%. This result seems advantageous when compared to the scarce works reported on heterogeneous catalytic oxidative cleavage of oleic acid. The organo-functionalization by optimized amount of CTA^+ could hydrophobically adjust the inherently hydrophilic surface of tungsten oxide giving more surface affinity to adsorb oleic acid in the reaction. This, together with the solid nature and insolubility of WO_x, provided the CTA^+-capped catalyst with additional advantages of no significant leaching of active sites, convenient recovery and steady reuse for up to four cycles without loss of activity. Hopefully, the application of this catalytic process could be extended to other UFAs available in vegetable oils, which would make diacids production more economical, commercially attractive, and environmentally friendly.

Acknowledgment

This work was supported by the Natural Science and Engineering Research Council of Canada (NSERC) through the INNOV-UC and Discovery grants. The authors wish to thank the industrial partners (Oleotek and SiliCycle Inc.) for stimulating discussions and comments.

5.5 Supporting Information

5.5.1 Characterization techniques

Powder X-ray diffraction (XRD) patterns of the samples were obtained on a Bruker SMART APEXII X-ray diffractometer equipped with a Cu Kα radiation source (λ = 1.5418 Å). Fourier transform infrared (FTIR) absorption spectra were measured with an FTS 45 infrared spectrophotometer with the KBr pellet technique. Thermo-gravimetric analysis (TGA) and differential thermal analysis (DTA) were performed with a TGA Q500 V20.13 Build 39 thermogravimetric analyzer from room temperature to 800 °C with a heating rate of 5 °C min^{-1} under an air flow of 50 mL min^{-1}. Transition electron microscopy (TEM) images were taken on a JEOL 6360 instrument at an accelerating voltage of 3 kV. Zeta potential was measured by means of a Zetasizer Nano 6 (Malvern Instruments Ltd) using a 4 mW He–Ne laser at 633 nm wavelength. The BET surface area was calculated by means of a Quantachrome Autosorb-1 system using N_2 adsorption-desorption isotherms at the temperature of liquid nitrogen and the data in the range of 0.05–0.3 P/P_0.

5.5.2 Analysis of the reaction products

Gas chromatography-mass spectrometry (GC-MS) analysis was used for the separation, identification, and quantification of the products after the reaction.

Fundamentally, fatty acids in their free form are difficult and fallible to analyze with GC, because these highly polar compounds tend to form hydrogen bonds with the stationary phase in GC columns, leading to adsorption issues. Reducing their polarity make them more amenable for analysis. Converting fatty acids to fatty acid methyl esters is the most common method for preparation of fatty acids prior to GC analysis, because methyl esters offer excellent stability, and provide quick and quantitative samples for analysis.

5.5.2.1 Sample preparation for GC-MS analysis

After a typical oxidative cleavage reaction, the products mixture underwent a derivatization reaction, in which the expectedly produced azelaic and pelargonic acids, and possibly unreacted

oleic acid were esterified to dimethyl azelate, methyl pelargonate, and methyl oleate, respectively. The esterification, briefly, involved heating the fatty acids in presence of an acid catalyst, boron trifluoride, in methanol to give fatty acid methyl esters. First, BF_3 protonates an oxygen atom of the carboxyl group making the acid much more reactive to nucleophiles, and then, methanol molecule combines with the protonated acid, to give the ester products. Scheme 5.1 shows derivatization mechanisms for oleic, azelaic, and pelargonic acids.

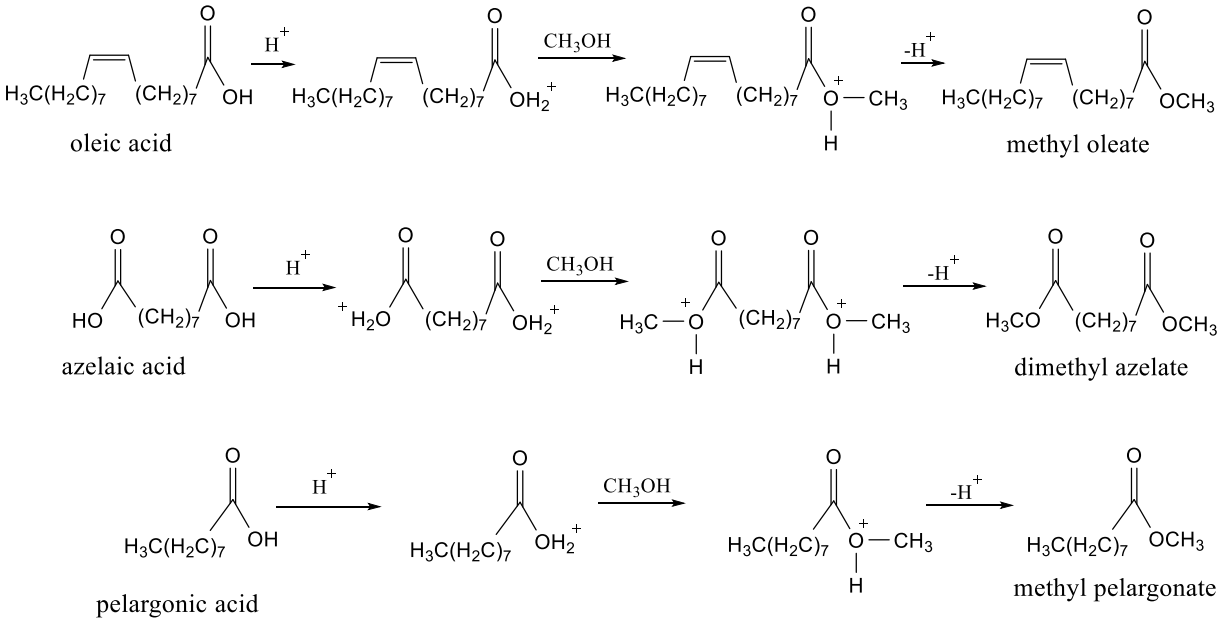

Scheme 5.1. Esterification of oleic, azelaic, and pelargonic acids with methanol to methyl oleate, dimethyl azelate, and methyl pelargonate, respectively, over an acid catalyst, BF_3.

Typically, BF_3-methanol (5 ml) (10% w/w, Sigma-Aldrich Co.) was, firstly, added to the fatty acids mixture, in which the total weight of fatty acids is less than 400 mg. Then, the mixture was heated to 80 °C for 15 min, followed by cooling down at room temperature for about 20 min. The ester products were extracted by adding 2 ml petroleum ether (Fisher Scientific Co.) and 2 ml water. After carefully removing the organic (upper) layer, the aqueous phase underwent the second extraction. Finally, the obtained organic phase was dehydrated by sodium sulfate (anhydrous, ≥99%, Sigma-Aldrich Co.) and then the solvent was removed by passing a steady stream of dry air. After properly dilution, the obtained esterified mixture was ready for injection to GC-MS.

5.5.2.2 Quantitative analysis

A typical derivatized sample, expectedly including dimethyl azelate, methyl pelargonate, and possibly methyl oleate, was injected to the GC-MS which had been previously calibrated by analytical standards of these methyl esters (all were purchased from Sigma-Aldrich Co.). A constant and exact amount of 1.0 μL was injected each time, and the injection was repeated at least four times for each sample to be averaged.

Obtained chromatograms of products for the catalytic tests, which their results have been presented in Table 5.2, entries 1-8, are shown in Figures 5.8-5.15 (Supporting Information). Owing to the carefully chosen column type and operating conditions of GC (see section 5.5.2.3), the obtained peaks had excellent shape and sharpness, which lead to reliable results. Based on peak areas in these chromatograms and the calibration curves of the standard methyl esters (which showed excellent linearity), conversion and yields of the oxidative cleavage reaction, reported in Table 5.2, were calculated (yield, in this work, was defined as number of moles of a product formed per mole of oleic acid consumed). Reproducibility of the results in this Table have been verified by performing at least 3 runs over each catalyst.

The properly adjusted temperature programming allowed separation of methyl pelargonate, dimethyl azelate, and methyl oleate with discrete retention times (R_t) of 10.4, 15.8, and 26.8 min, respectively. Some other peaks were also observed in the chromatograms, indicating presence of by-products, which were qualitatively analyzed by MS, as follows. Small and often negligible peaks in e.g. R_t= 6.8, 8.9, 11.2, and 16.7 min belonged to octanal, methyl esters of hexanoic and octanoic acids, and 9,10-dihydroxy octadecanoic acid, respectively, which were produced by impurities of the reactants and/or insignificant side reactions (e.g. hydroxylation). Two relatively more considerable peaks in R_t= 8.6 and 13.8 min belonged to nonanal and 9-oxononanoic acid, respectively, which were produced by partial-oxidation of oleic acid. Since after minute 30 no significant peak was obtained, the chromatograms in Figures 5.8-5.15 have been monitored up to R_t= 30 min.

It should be noted that such by-products like 9-oxononanoic acid, which are the direct result of involvement of carboxylic group in the reaction, has made oxidative cleavage of unsaturated

fatty acids, compared to alkenes and cyclic olefins, more complicated and investigation of their reaction mechanism more difficult. It makes more sense given the fact that 9-oxononanoic acid is not commercially available (in known chemical provider companies), which makes calibration of chromatography systems by the analytical standard of this chemical, and consequently its quantitative analysis by these systems impossible.

Further kinetic studies are underway in our laboratory to investigate the competition between partial and over-oxidation of oleic acid and propose a mechanism indicating how both oleic acid and hydrogen peroxide are activated by the synthesized catalysts.

5.5.2.3 GC-MS specifications

The GC-MS included a Hewlett-Packard HP 5890 series GC system and MSD Hewlett-Packard model 5970. GC system was equipped with Zebron ZB-5MS capillary column (30 m × 0.25 mm × 0.25 mm). Helium was used as a carrier gas with the flow rate of 30 mL/min. A split ratio of 20:1 was fixed. The front inlet temperature was 280 °C. The oven temperature program consisted of maintaining at 50 °C for 2 min, then a ramp rate of 10 °C/min to 160 °C following by a hold-up time of 1 min, and further increase with the rate of 5°C/min to 290 °C. Direct injection by a 5.0 µL syringe (SGE fixed needle, 23-26 gauge/42mm L/Cone Tip, Phenomenex Co.) was employed with 1.0 µL injection amount for each run. HP Chemstation software was used to analyze data.

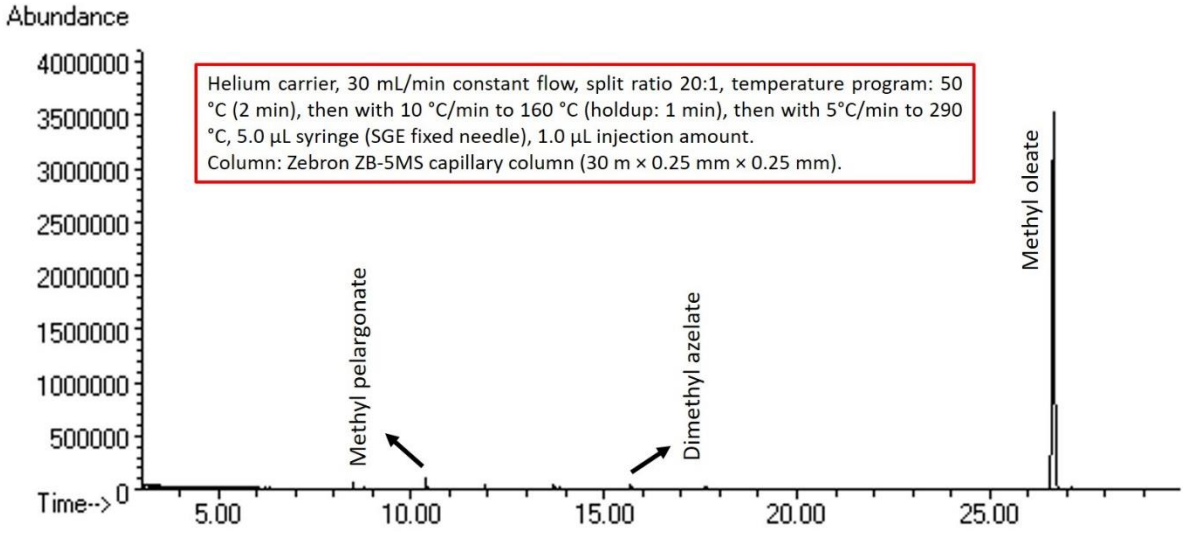

Figure 5.8. Gas chromatogram of products of the catalytic test in absence of catalyst (entry 1, Table 5.2).

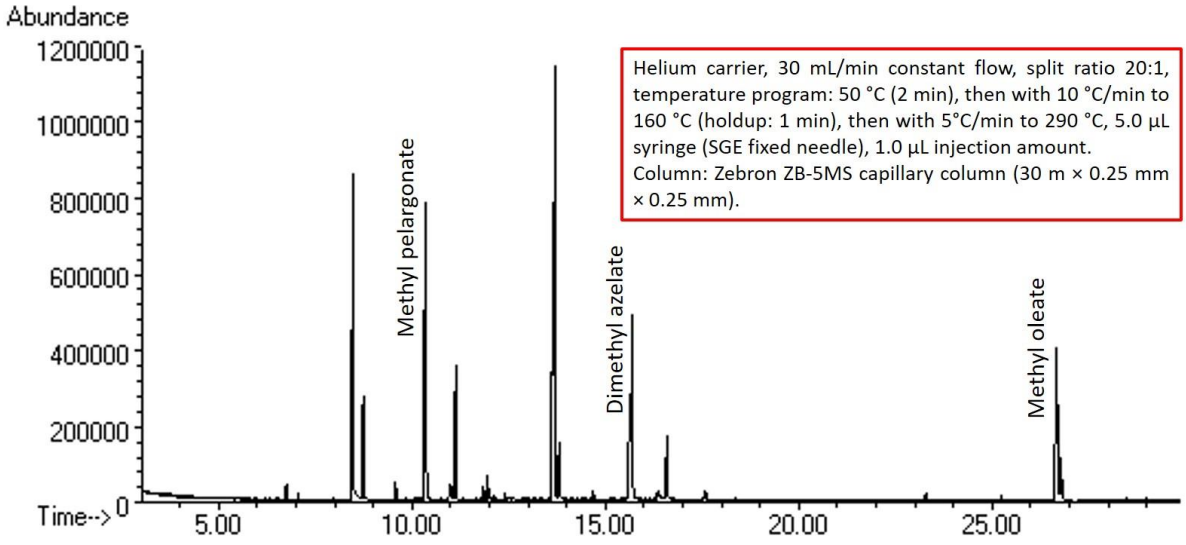

Figure 5.9. Gas chromatogram of products of the catalytic test over commercial tungsten oxide (entry 2, Table 5.2).

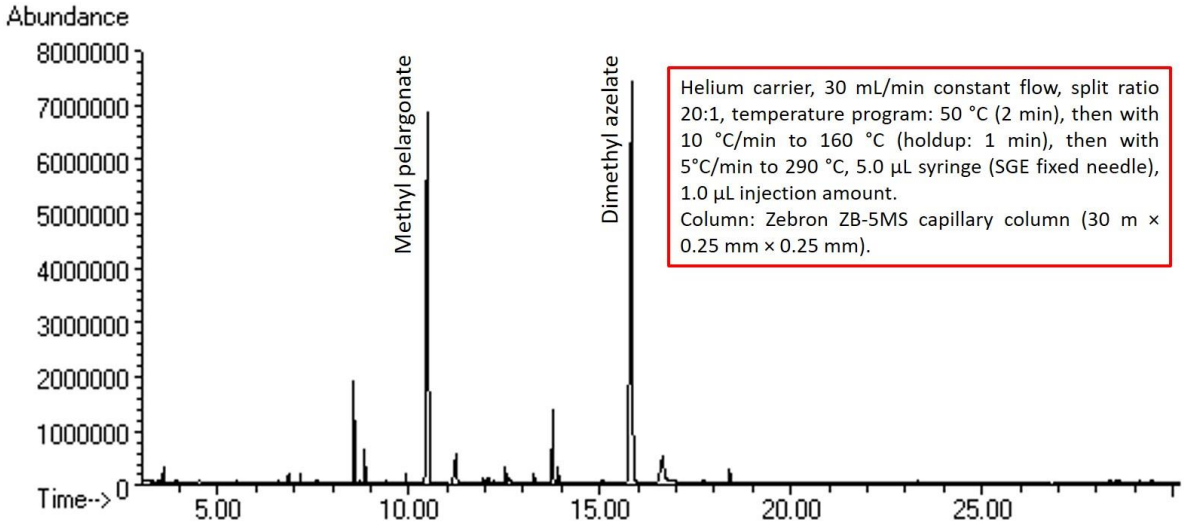

Figure 5.10. Gas chromatogram of products of the catalytic test over sample I (entry 3, Table 5.2).

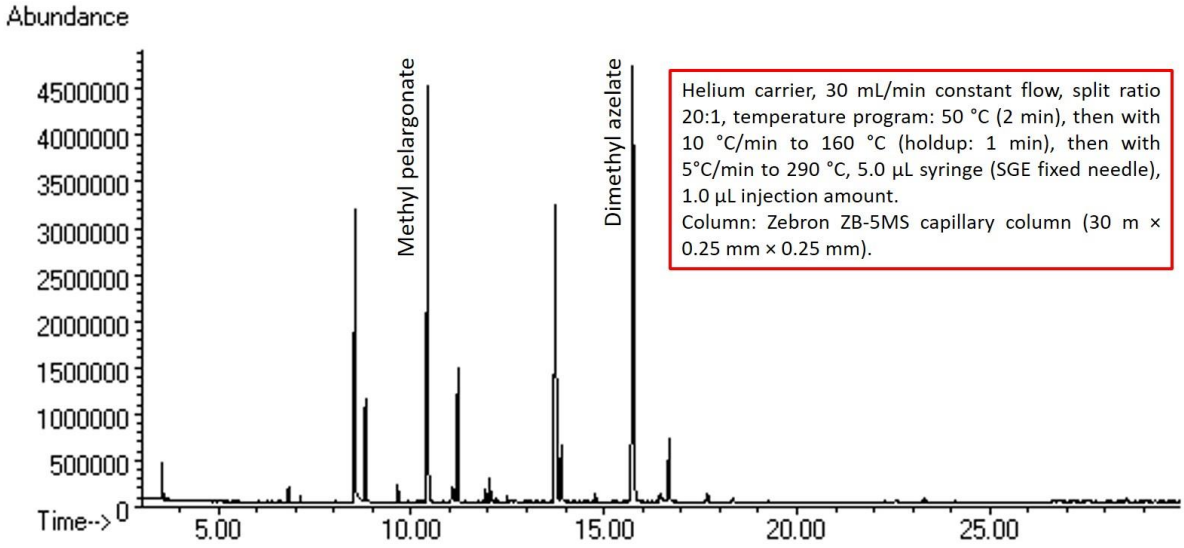

Figure 5.11. Gas chromatogram of products of the catalytic test over sample II (entry 4, Table 5.2).

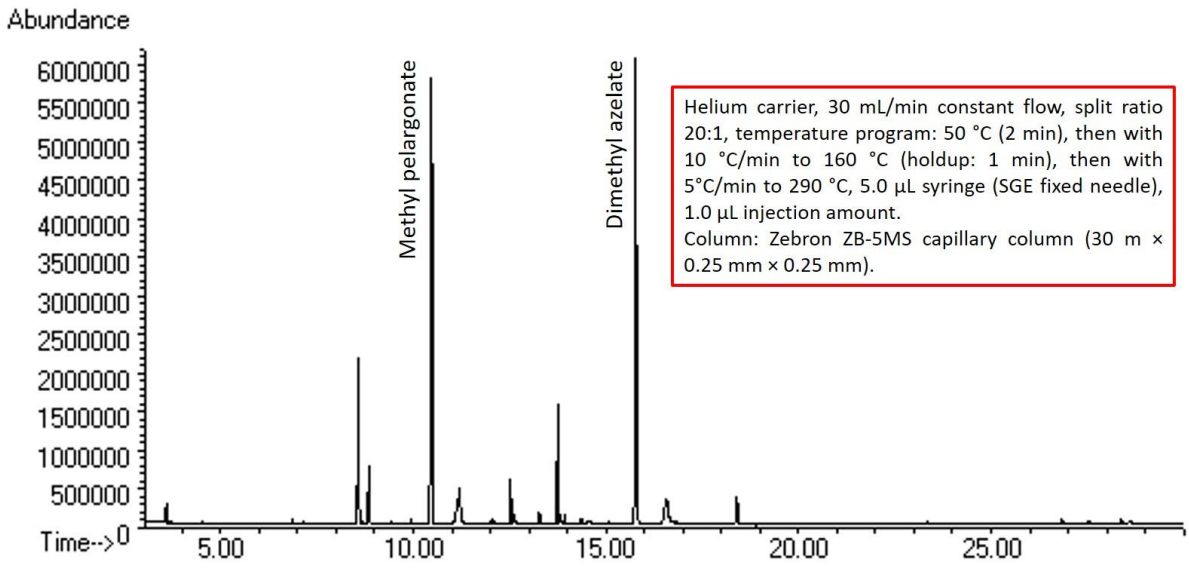

Figure 5.12. Gas chromatogram of products of the catalytic test over sample III (entry 5, Table 5.2).

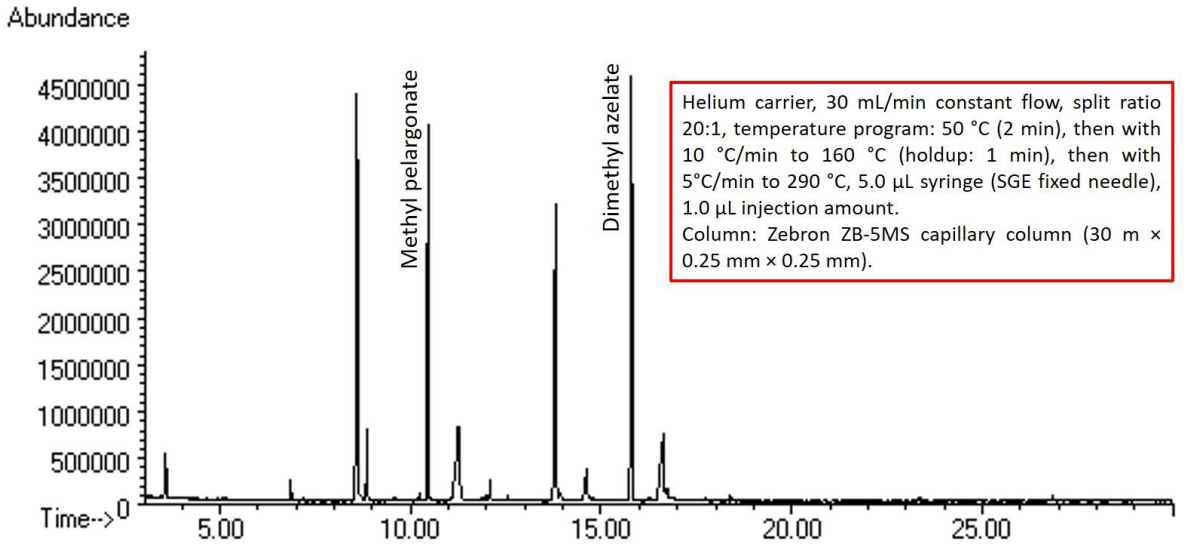

Figure 5.13. Gas chromatogram of products of the catalytic test over sample IV (entry 6, Table 5.2).

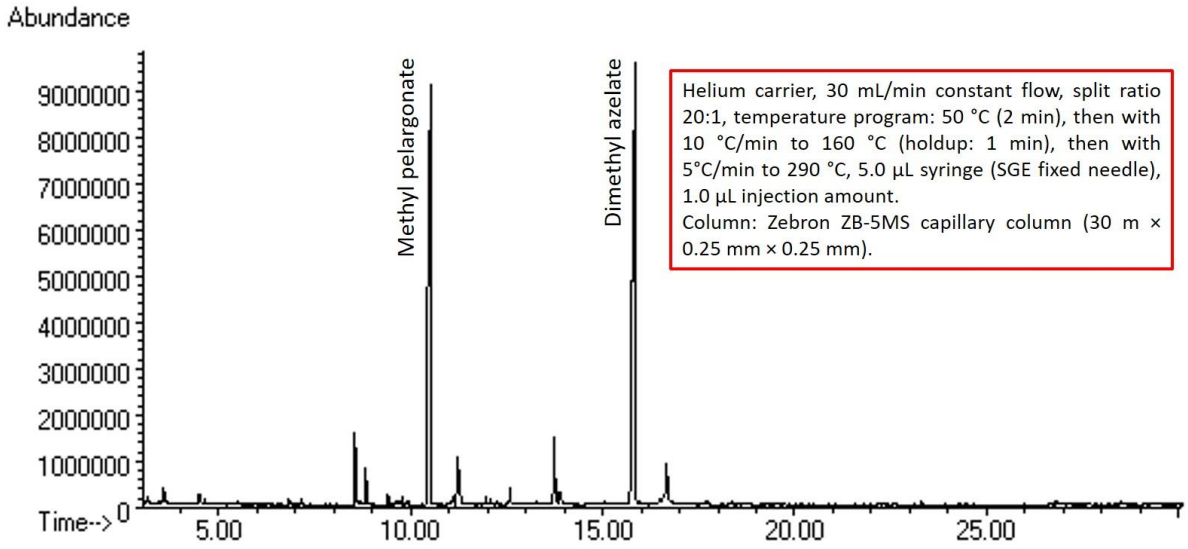

Figure 5.14. Gas chromatogram of products of the catalytic test over sample V (entry 7, Table 5.2).

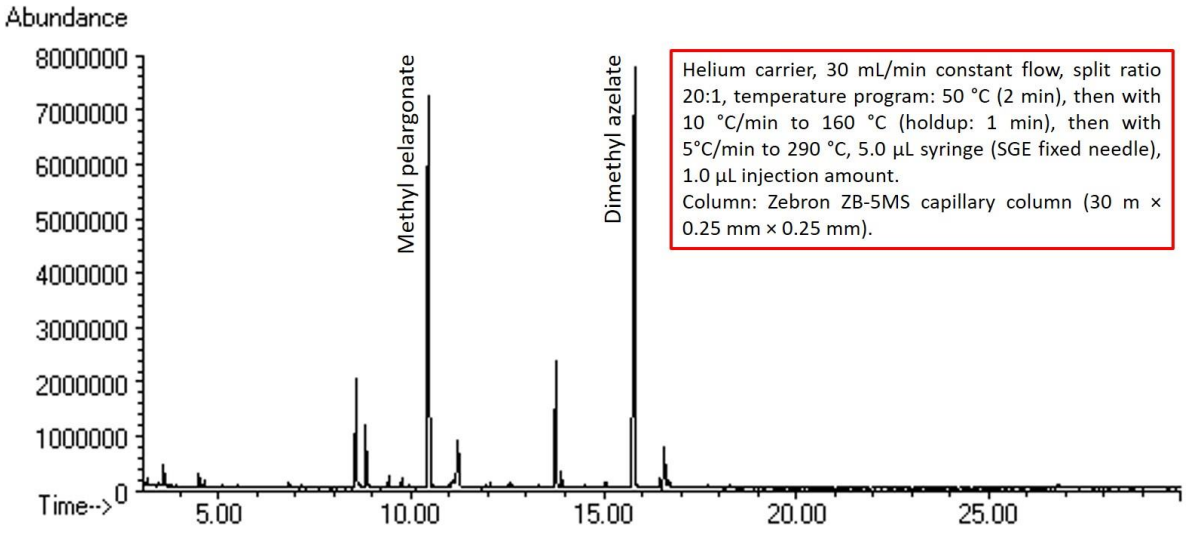

Figure 5.15. Gas chromatogram of products of the catalytic test over sample VI (entry 8, Table 5.2).

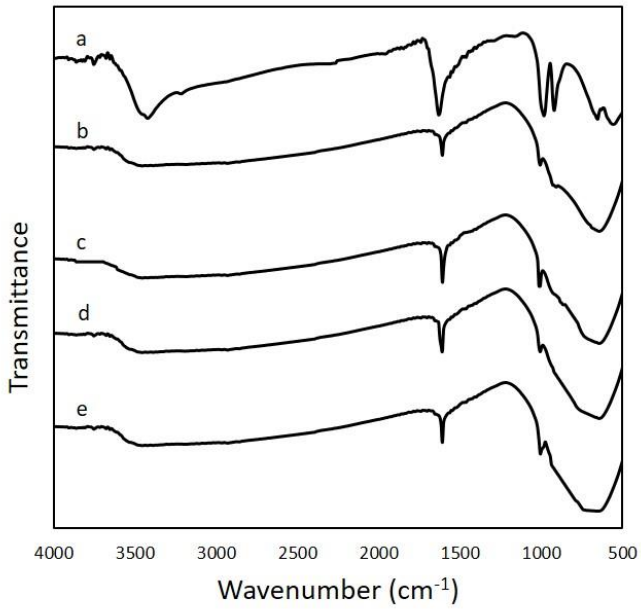

Figure 5.16. FTIR spectra of sample I: (a) before reaction, (b) after 1st cycle, (c) after 2nd cycle, (d) after 3rd cycle, and (e) after 4th cycle.

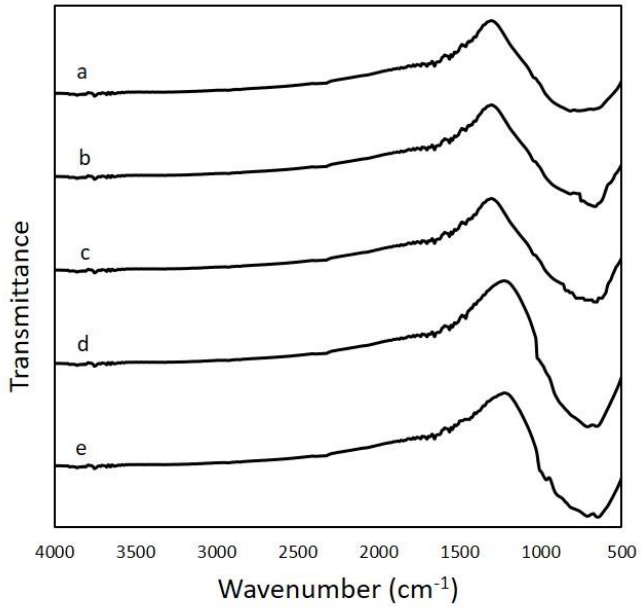

Figure 5.17. FTIR spectra of sample II: (a) before reaction, (b) after 1st cycle, (c) after 2nd cycle, (d) after 3rd cycle, and (e) after 4th cycle.

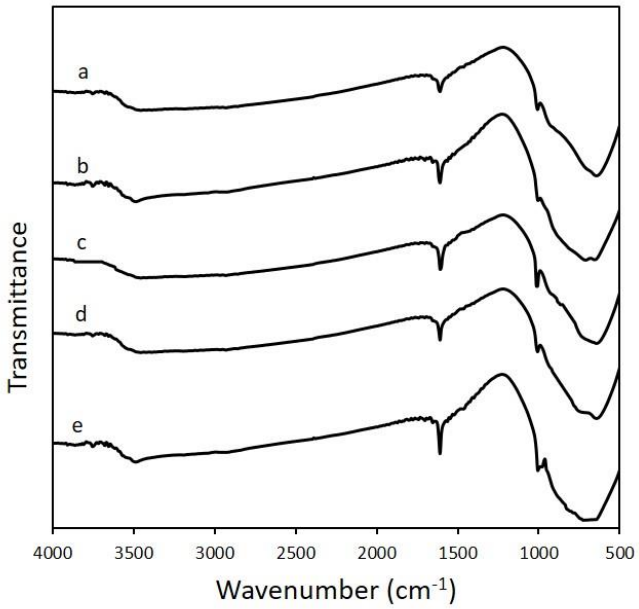

Figure 5.18. FTIR spectra of sample III: (a) before reaction, (b) after 1st cycle, (c) after 2nd cycle, (d) after 3rd cycle, and (e) after 4th cycle.

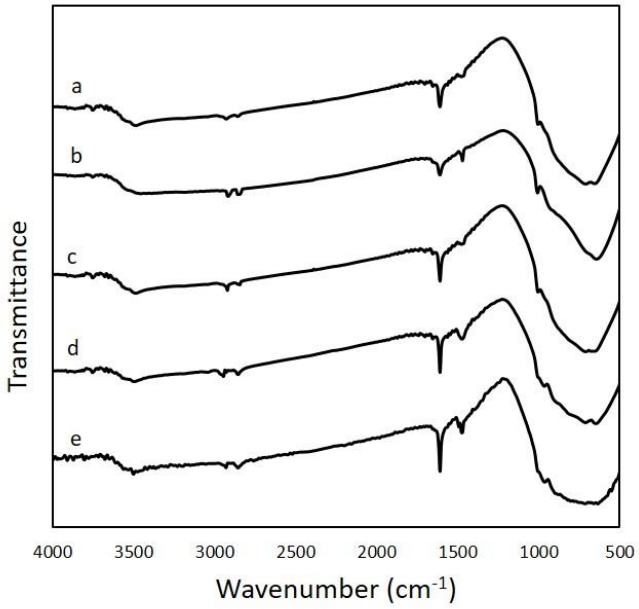

Figure 5.19. FTIR spectra of sample IV: (a) before reaction, (b) after 1st cycle, (c) after 2nd cycle, (d) after 3rd cycle, and (e) after 4th cycle.

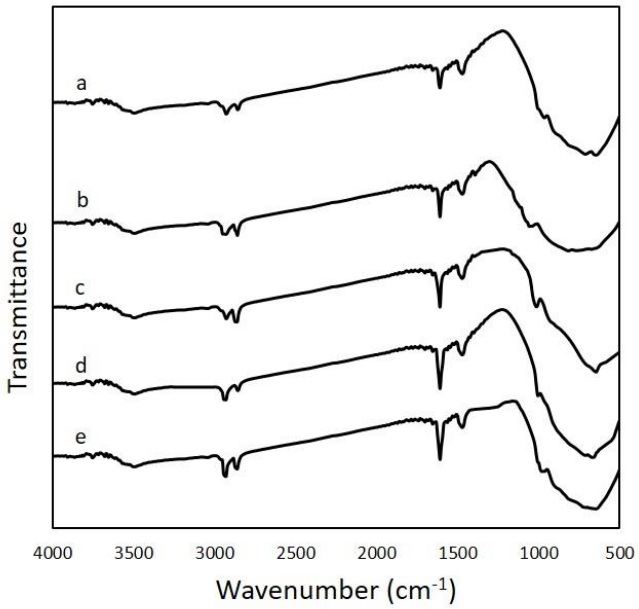

Figure 5.20. FTIR spectra of sample V: (a) before reaction, (b) after 1st cycle, (c) after 2nd cycle, (d) after 3rd cycle, and (e) after 4th cycle.

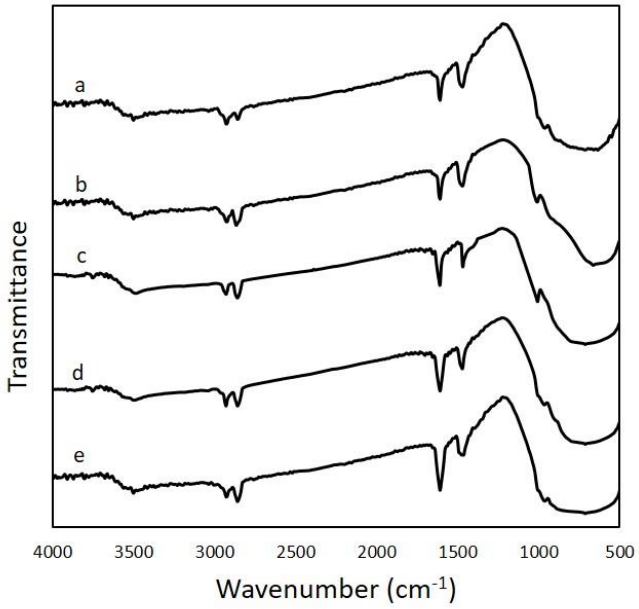

Figure 5.21. FTIR spectra of sample VI: (a) before reaction, (b) after 1st cycle, (c) after 2nd cycle, (d) after 3rd cycle, and (e) after 4th cycle.

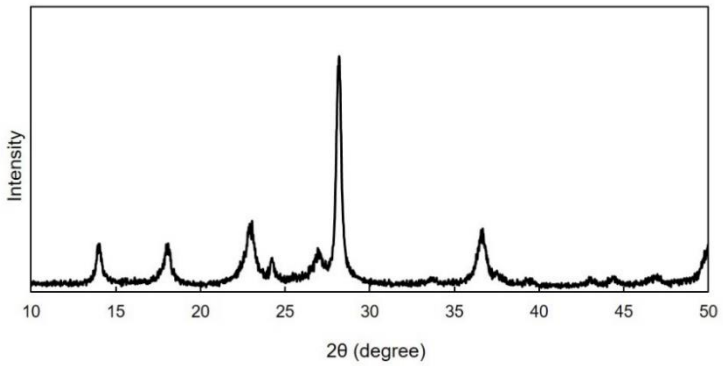

Figure 5.22. XRD pattern of sample I after reaction; $WO_3.0.33H_2O$ (PDF no. 87-1203).

Table 5.3. Assignments of the FTIR absorption bands of the prepared samples [369].

Sample	Absorption bands (cm^{-1})	Assignment
I	548	W (O_2)
	649	ν (W-O)
	919	ν (O-O)
	981	ν (W=O)
	1622	δ (H-O-H)
	3421	ν (H-O-H)
II	672	ν (W-O)
III	641	ν (W-O)
	1004	ν (W=O)
	1606	δ (H-O-H)
	3452	ν (H-O-H)
IV	649	ν (W-O)
	973	ν (W=O)
	1467	$RN(CH_3)_3^+$
	1606	δ (H-O-H)
	2850, 2927	ν (CH_3 and/or CH_2)
	3491	ν (H-O-H)
V	641	ν (W-O)
	958	ν (W=O)
	1467	$RN(CH_3)_3^+$
	1606	δ (H-O-H)
	2850, 2927	ν (CH_3 and/or CH_2)
	3491	ν (H-O-H)
VI	656	ν (W-O)
	950	ν (W=O)
	1467	$RN(CH_3)_3^+$
	1606	δ (H-O-H)
	2850, 2927	ν (CH_3 and/or CH_2)
	3491	ν (H-O-H)

Table 5.4. BET surface areas of the synthesized samples.

Sample	CTAB/W molar ratio	S_{BET} (m^2/g)
I	-	8.6
II	-	29.1
III	-	17.0
IV	0.1	14.0
V	0.25	7.8
VI	0.5	4.3

Table 5.5. Weight losses of the synthesized catalysts during the different cycles of the reaction.

Reaction cycle	Sample I	Sample II	Sample III	Sample IV	Sample V	Sample VI
1st	2.1	1.3	1.8	1.4	1	0.8
2nd	2	1.7	1.6	1.4	1.2	0.9
3rd	1.9	1.2	1.4	1.3	1.3	1
4th	2	1.6	1.7	1.5	1.4	1